Hou, R.-Q.; Scharnagl, N.; Feyerabend, F.; Willumeit-Roemer, R.:
Exploring the effects of organic molecules on the degradation of magnesium under cell culture conditions
In: Corrosion Science 132 (2018) 35 - 45
First published online by Elsevier: December 20, 2017

DOI: 10.1016/j.corsci.2017.12.023
https://dx.doi.org/10.1016/j.corsci.2017.12.023

Exploring the effects of organic molecules on the degradation of Magnesium under cell culture conditions

Rui-Qing Hou [a], Nico Scharnagl [a], Frank Feyerabend [a*], Regine Willumeit-Römer [a]

[a] Helmholtz-Zentrum Geesthacht, Institute of Material Research, Max-Planck-Str. 1, 21502 Geesthacht, Germany

[*] Corresponding author:

Dr. Frank Feyerabend, Phone: +49 (0)4152 871259, Fax: +49 (0)4152 872595,

E-mail: *frank.feyerabend@hzg.de*

Abstract: Several typical organic components, L-ascorbic acid (L-AA), L-glutamine (L-Gln), L-alanyl-L-glutamine (L-Ala-L-Gln) and fetal bovine serum (FBS) were chosen to elucidate the effects of organic components on the degradation of pure Mg under cell culture conditions. The results revealed that the influence of organic components on the degradation of pure Mg is time-dependent and they play an important role in the formation of the degradation layer. The addition of organic components favors the precipitation of nesquehonite rather than hydromagnesite in the "outer" layer, while in the "inner" layer the organic components accelerates the formation of phosphate (Mg-PO_4, Ca-P salts) during immersion.

Keywords: IR spectroscopy; XRD; amorphous structures; interface; kinetic parameters

Funding: This work was supported by the Helmholtz Virtual Institute "In vivo studies of biodegradable magnesium based implant materials (MetBioMat)" (grant number: VH-VI-523). China Scholarship Council (CSC) provides financial support for RQH. The funders had no role in study design, data collection and analysis, decision to publish, or preparation of the manuscript.

Conflicts of interest: The authors declare no conflict of interest.

Authors' contribution: Conceived and designed the study: RQH and FF. Performed the experiments: RQH and NS. Contributed reagents/materials/analysis tools: NS, FF and RW. Analysed and discussed the data: RQH, NS, FF and RW. Wrote the paper: RQH. Reviewed and edited the manuscript: NS, FF and RW. All authors read and approved the manuscript.

1. Introduction

Magnesium (Mg) alloys have become more and more favorable in medical applications due to their excellent biodegradability and bioresorbability [1-3] and clinical applications are already reported [4]. However, a too high, in some cases unpredictable, degradation rate is still a problem for their applications because it can lead to the formation of gas pockets, high ionic concentrations and pH which result in the failure of implant in the early service [5-7]. Therefore, the establishment of a reliable evaluation standard is a prerequisite for their application as absorbable metallic implants with controllable degradation speed.

For the successful establishment of this reliable evaluation standard, it is necessary to evaluate the effect of physiological parameters on the degradation of Mg-based biomaterials. Many degradation studies have been conducted in simple to complex salt solutions, such as Hank's solution and simulated body fluid (SBF), to investigate the influence of inorganic ions on the degradation of Mg alloy [8-13]. The impurities of materials (for example Fe) is also very important for Mg degradation due to the enhancement of galvanic corrosion [14]. Additionally, the pH buffering of media and the temperature used for *in vitro* tests always affect the Mg degradation [15]. Chloride ions (Cl^-), as the most important part, largely accelerate the degradation of Mg implants by breaking the integrity of the surface film [8, 10, 16], phosphates decrease the degradation rate due to the formation of dense phosphate layer [8], and an appropriate amount of carbonate ions can induce rapid surface passivation because of the precipitation of magnesium carbonate [8, 9]. The monovalent cations (K^+, Na^+) in solution are more prone to accelerate the degradation of Mg than divalent cations (Ca^{2+}, Mg^{2+}) [12]. However, these simple salt solutions under normal conditions are far away from the real physiological environment which comprises a very complex mixture of organic and inorganic

molecules and a different concentration of O_2/CO_2 at different implant sites, which results in the difference between *in vitro* and *in vivo* degradation [17, 18].

Consequently, the inclusion of organic components in simulated solutions is the next step towards a closer simulation of *in vivo* conditions and a better understanding of the degradation of Mg alloys. Therefore, cell culture media containing amino acids and vitamins, such as Dulbecco's modified Eagles' medium (DMEM) and minimum essential medium (MEM), have already been used for the degradation tests under cell culture conditions. These organic components significantly altered the degradation behavior of Mg due to the chelating/binding effect and the adsorption of organic molecules on Mg surface [15, 19-23]. Furthermore, the adsorption of proteins has been used to develop protective films for the controllable degradation of Mg alloys [24-26]. On the other hand, organic components also affect the formation of the degradation layer during immersion. For example, proteins can adsorb on the Mg surface, thereby leading to the variation of the surface layer compactness or thickness [27, 28]. Some conditions also result in the severe deposition of precipitates on the surface, resulting in two sections of the degradation layer: loosely "outer" crystalline layer and "inner" amorphous layer [29]. In different media, the organic components also show different influence on the formation of degradation products. In HBSS, the addition of fetal bovine serum (FBS) postponed the formation of "outer" crystalline products, while the formation of Ca-P salts was promoted by FBS in simulated body fluid (SBF) [30]. However, the influence of organic components on the degradation of Mg had not reached a consensus due to the complicated system when organic components were added and their complexity in chemical reactions with the environment. Moreover, reliable *in vitro* evaluation standards for absorbable Mg have been neither established nor compared with *in vivo* tests. Therefore, it is of great significance to have insight into the effects of organic components on the degradation of Mg.

The aim of this study is to examine the effects of several typical organic components used in cell culture media on the degradation of Mg. A simple salt solution, Hank's balanced salt solution (HBSS) without calcium and magnesium, was used as the base solution. L-ascorbic acid (L-AA), L-glutamine (L-Gln), L-alanyl-L-glutamine (L-Ala-L-Gln) and fetal bovine serum (FBS) were chosen to elucidate the influence of organic components on the degradation process. L-AA (vitamin C) is one of the most important vitamins in human body, which enhances the immune system and prevents various oxidative stress-related diseases, such as cancer and cardiovascular diseases [31, 32]. L-Gln is the most abundant free amino acid in human body with the largest storage area in skeletal muscle [33]. It is involved in many physiological functions including cellular proliferation, acid-base balance, antioxidant synthesis and protein synthesis in the muscle [34-38]. However, L-Gln is unstable in solution during heat sterilization and prolonged storage, thereby deaminating into ammonia which has deleterious effects on cells [39]. Therefore, L-Ala-L-Gln as a dipeptide is used as a substitute for L-Gln in cell culture media. It is less ammoniagenic than L-Gln, which contributes to its advantages as a media component [40]. By using these four organic components, the effects of organic components on the degradation of pure Mg were investigated by analyzing the changes of media during immersion and the degradation layers formed in different media.

2. Materials and Methods

2.1. Materials

Pure Mg (99.94 %, chemical composition is shown in Table 1) used in this study was purchased from Magnesium Elektron (Manchester, UK). Rectangular specimens with dimensions of 10 mm × 10 mm × 4 mm were cut out of the ingots via arc erosion (AMS tech., Taiwan). Before use, the specimens were successively wet ground with SiC abrasive paper (Schmitz-Metallographie GmbH,

Herzogenrath, Germany) from 800 to 2500 grit, then ultrasonically cleaned for 20 min in N-hexane, 5 min in acetone and 20 min in ethanol (Merck KGaA, Darmstadt, Germany). Finally, the samples were dried in 12-wells cell culture plates (Greiner Bio-One, Frickenhausen, Germany) for at least 30 min in air under sterile conditions. The homogeneity of materials has been investigated by characterizing the microstructure and surface roughness before the immersion tests, the representative results were supplied in supplement files (Fig. s1).

2.2. Immersion media

Hank's balanced salt solution (HBSS, Order-No. 14715, Life Technologies, Darmstadt, Germany) without calcium and magnesium addition (the composition is shown in Table 2), was used as a base solution for all immersion media. L-AA (Sigma-Aldrich Chemie, Steinheim, Germany), L-Gln (Thermo Fisher, Karlsruhe, Germany), L-Ala-L-Gln (Biowest, Darmstadt, Germany) and 10 % FBS (PAA laboratories, Linz, Austria) as a protein component, were added in a concentration comparable to that in two cell culture media, Dulbecco's modified Eagle's medium (DMEM) and Minimum Essential Media Alpha (α-MEM). After these components except FBS were added into HBSS, the media were sterile filtered by bottle top-filters with a pore size of 0.2 μm (Thermo Fisher, Karlsruhe, Germany). Thus, eight immersion media were prepared as following:

A: Base solution (HBSS)

B: HBSS + 50 mg/L L-AA

C: HBSS + 292 mg/L L-Gln

D: HBSS + 862 mg/L L-Ala-L-Gln

E: HBSS + 50 mg/L L-AA + 292 mg/L L-Gln

F: HBSS + 50 mg/L L-AA + 862 mg/L L-Ala-L-Gln

G: HBSS + 50 mg/L L-AA + 292 mg/L L-Gln + 10 % FBS

H: HBSS + 50 mg/L L-AA + 862 mg/L L-Ala-L-Gln + 10 % FBS

2.3. Immersion test

Before sterilization, the initial weights of samples as well as the initial pH (SENTRON ARGUS X pH-meter, Fisher Scientific, Schwerte, Germany) and osmolality (Osmomat 030, Gonotec, Berlin, Germany) for the eight immersion media were recorded. Eighteen samples were immersed in media as a sample weight to medium volume ratio of 0.2 g/mL under cell culture conditions (37 °C, 5 % CO_2, 20 % O_2, 95 % rel. humidity) in an incubator (Heraeus BBD 6620, Thermo Fisher Scientific, Schwerte, Germany). The immersion media were changed every 2 or 3 days to present a semi-static immersion test. pH and osmolality were determined after each change of the media. Media without samples were incubated in parallel as controls.

A 24-well Sensor Dish with integrated sensor spots at the bottom of each well (PreSens Precision Sensing GmbH, Regensburg Germany) was used to monitor the change of pH with the immersion time. The concentration of L-Gln in media was determined by using the glutamine colorimetric assay kit (BioVision, Inc., Zürich, Schweiz). The standard curve was prepared by using Gln standard solutions with a successive concentration from 0 µM to 250 µM. At each time point, 10 µL of media with or without samples (three replicates) were taken out from well plates, then centrifuged at 10000 g for 5 min at 4 ˚C. 2 µL of the supernatant was added to 96-well clear plates with flat bottom. The volume was adjusted to 40 µL/well with ddH_2O. 10 µL hydrolysis mix solution was added to each sample well, then the plates were incubated for 30 min at 37 ˚C. Subsequently, 50 µL reaction mix solution was added to each sample well. The plates were incubated for 60 min at 37 ˚C. Finally, the absorbance at 450 nm was measured with a reference absorbance at 620 nm in Tescan A-5082 microplate reader (Sunrise Romote, Austria).

2.4. Degradation rate

Six samples were taken out of the respective media at the time points of 3 days, 7 days and 14 days, then cleaned twice with double distilled water and dried at 50 °C in air. Two samples were left to analyze the surface product and prepare the cross section. Degradation products on other four sample surfaces were removed by immersion in chromic acid (180 g/L chromium (VI) oxide in distilled water, VWR International, Darmstadt, Germany) for 20 min at room temperature. Afterwards they were rinsed in distilled water and 100 % ethanol. After drying, the weights of the samples were determined again and the mean degradation depth (h) in μm was calculated according to the equation:

$$h = \frac{10000 \cdot \Delta m}{A \cdot \rho} = \frac{DR \cdot t}{8.76} \qquad (1)$$

where A is the surface area in cm^2, ρ is the density of pure Mg (1.74 g/cm^3), t is immersion time in hours, Δm is the observed mass loss in gram and DR is the degradation rate in mm/year. The degradation expression by using mean degradation depth has a higher probability in determining the realistic degradation rates of Mg alloys, especially for the long-term immersion, and the rationality has been discussed in literature [41]. To compare with other reports, the transformation between h and DR also was listed in equation (1). For example, the mean degradation depth after 3 day immersion in HBSS is 22.87 ± 1.39 μm, which is equivalent to the degradation rate of 2.78 ± 0.17 mm/year.

Prior to the use of chromic acid, the ground samples without immersion were treated with chromic acid for 20 min to investigate the influence of chromic acid on the bulk materials (pure Mg). The same weight of samples before and after treatment with chromic acid indicates that chromic acid treatment will not dissolve the bulk materials (pure Mg).

2.5. Surface morphology

The samples after different days of immersion without further treatment were used directly to check the morphology by scanning electron microscopy (SEM, Phenom-World, Eindhoven, Netherlands) in backscattering mode with an accelerating voltage of 15 kV.

2.6. Degradation products analysis

In this study, the degradation layer or degradation products refer to both "inner" amorphous products and "outer" crystalline products unless the nomenclature for this layers is in the following "inner" and "outer". To identify the products formed and deposited on the surface, the Mg surfaces after different days of immersion without further treatment were examined by X-ray diffraction (XRD), performed on a Bruker D8 Advance (Bruker, Karlsruhe, Germany) in grazing incidence geometry at an incident angle of 3 °. The generator was set for 40 kV and 40 mA. Data was collected between 2θ = 10 ° - 70 ° at 0.01 ° intervals. The counting time was 0.5 s per data point. Data analysis was carried out using analysis software (BrukerEVA and PDF-2 Release 2015 RDB).

To detect the composition of the "inner" degradation products, the "outer" precipitates on the surface were removed as much as possible with adhesive tape. The samples were investigated by SEM (Phenom-World, Eindhoven, Netherlands) to confirm the removal of the precipitates prior to the characterization by infrared spectroscopy in reflectance mode. Then a Bruker Tensor 27 infrared spectrometer equipped with an infrared microscope (Bruker Hyperion 2000, Ettlingen, Germany) was used to record the absorbance spectra of degradation products formed on the Mg surface from different media. The spectra were recorded with a resolution of 2 cm^{-1}, taking 512 scans. For data evaluation Brukers OPUS software version 7.5.18 was used.

2.7. Composition of degradation layer

Before the removal of "outer" precipitates layer, the cross sections of samples were prepared by embedding in resin (Demotec 30, Nidderau, Germany), with the cross sections oriented upwards and subsequently polished with colloidal silica suspension (Cloeren Technology GmbH, Wegberg, Germany) to a mirror-like surface. The resulting surfaces were analyzed by backscattered electron (BSE) images of the degradation layer, and chemical element mapping by utilizing a scanning electron microscope (Tescan Vega3 SB, Brno, Czech Republic) equipped with energy dispersive spectrometer (EDS) was conducted. At least 80 sites of cross section for each sample were measured for the layer thickness from the BSE images. Element mappings were performed using an accelerating voltage of 15 kV and the resolution was 256 pixels. The diameter of beam was 300-500 nm depending on the beam intensity used. The acquisition time was 80 ms per pixel. The area of the scanned surface depended on the magnification used. The pixel size was about 400 nm × 400 nm. The nominal acceleration depth for Mg is at least about 3.5 μm under this condition. The minimum limit of detection in our experiments was 1000 ppm. The deviation of counting statistics is 3-6 %. The weight percentages of phosphorus in degradation products near the Mg matrix were calculated from the mapping by using Iridium Ultra software.

2.8. Statistical analysis

The data were analyzed and plotted using the software Origin 9.0 (Originlab Corporation, Wellesley Hills, USA). Standard analysis comparing more than two treatments was done by using one-way analysis of variance (ANOVA) on ranks with Dunn's multiple comparison post hoc tests. Figs. 4, 7, 9 were organized by using Adobe Photoshop CS6 (Adobe Systems Incorporated, San Jose, USA).

3. Results

3.1. Degradation depth, pH, osmolality and layer thickness

The mean degradation depths of pure Mg after 3, 7 and 14 days of exposure in different media are depicted in Fig. 1. After 3 days of immersion, there was no significant difference between the mean degradation depths in different media. However, after a relatively long immersion (14 days), the samples immersed in media with organic components showed a higher degradation depth than the control (in HBSS), especially for those in media with more than one kind of organic components.

The changes in pH and osmolality of the degradation media were measured during each change of media, as shown in Fig. 2. As expected, both the pH and the osmolality changed to higher values irrespective of the used media compared to those without samples. The increase in pH was generally higher for HBSS than other media, while the increase in osmolality showed an adverse trend, especially for the media with more than one kind of organic components. The osmolality of all media generally decreased with incubation time, suggesting the decrease of degradation rates with immersion time.

Generally, the thickness of the degradation layer tended to increase with the incubation time (Fig. 2c). Single organic components, like L-AA, L-Gln, L-Ala-L-Gln, led to thickening of the degradation layer. In contrast, when more than one kind of organic components was present, the layer thickness sharply decreased compared with that formed in HBSS.

3.2. The concentration of L-Gln during immersion

To verify the participation of L-Gln in the formation of degradation products, the concentration of L-Gln was measured during the incubation as shown in Fig. 3b. Since L-Gln is not stable during incubation and it could deaminate with the increase of pH, pH of media were also determined during the incubation (Fig. 3a). The range of the on-line pH device (pH: 5~9) limited the determination of

pH, which led to a vacancy during the first several hours of immersion. However, it could be seen that pH reached stable values after about 20 hours of immersion. The concentrations of L-Gln also were measured at different pH (Fig. 3b), it was stable at around 1.4 mM, which indicated after 20 hours of immersion the deamination of L-Gln had little influence on the concentration of L-Gln. However, the concentration of L-Gln with samples decreased after 20 hours' incubation, suggesting L-Gln participated in the process of degradation by adsorption or other ways.

3.3. Surface morphology

All samples after immersion showed a blackish surface with some white precipitates (the optical images can be seen in Fig. s2 of the supplementary). A comparison of the sample surfaces after degradation is shown in Fig. 4. From the SEM images, the white precipitates in HBSS and HBSS with one kind of organic components showed a conglomerate of very thin platelets. When two kinds of organic components were added in HBSS, a well-formed needle-like precipitate layer was present on the surface. However, the needles gradually diminished with the immersion time, suggesting the needles were not stable under this condition. The addition of FBS had further influence on the morphology of the precipitates on the surface. The detailed morphologies are shown in the images with a high magnification (Fig. 4).

3.4. The composition of degradation products

Since the samples with same morphology had a reproducible spectrum, typical spectra of the degradation layer with different morphology were selected to present the XRD results. As shown in Fig. 5, the results revealed that hydromagnesite (reference card 00-070-1177) and dypingite (reference card 00-29-0857 and 00-23-1218) were the main components of the conglomerate composed of thin platelets, while the well-formed needles were nesquehonite (reference card 00-020-0669). The precipitates formed in HBSS containing FBS are also nesquehonite, although the

morphology of precipitates changed after the addition of FBS (Fig. 4). However, after the removal of the "outer" precipitates, the morphology of the "inner" degradation layers formed in different media showed little difference (SEM images in Fig. 5). The XRD patterns only had several weak peaks from Mg, suggesting the amorphous state of the "inner" degradation products or the nanocrystals formed in the "inner" layer.

To give an insight into the composition of the "inner" degradation layer, IR reflection spectra were conducted for the samples after the removal of the "outer" precipitates by adhesive tape. The spectra from the surface of the "inner" degradation layer formed in different media gave similar information, indicating similar components of all "inner" degradation layers. Therefore, typical examples are given in Fig. 6 (the spectra of samples in different media are all provided in Fig. s3). Strong IR signals in the range 1400-1550 cm^{-1} arise from the anti-symmetrical CO_3^{2-} stretching and/or amide II of organic components [25, 28], while the band at 860 cm^{-1} is assigned to the CO_3^{2-} bending vibration [42]. The shoulder at 1640 cm^{-1} is ascribed to an OH-bending mode of water and/or amide I of organic molecules [8]. The broad band centered near 3500 cm^{-1} is attributed to the stretching vibration of the hydroxyl group. This broad band stems mainly from strong H bonding of water inside the "inner" degradation products, which absorbed on the degradation products or embedded in interstitial spaces of degradation products [13]. The band around 1050 cm^{-1} is associated with the asymmetric stretching of phosphate [43]. Moreover, a weak sharp band at 3698 cm^{-1} is related to the free hydroxyl group, indicating the presence of $Mg(OH)_2$ in the "inner" layer [42]. Therefore, it can be confirmed that the "inner" degradation products were mainly magnesium carbonate, phosphate and magnesium hydroxide. Most probably MgO also is present, as previously proposed [44]. MgO could not be detected in our experiments due to the high signal to noise ratio below 600 cm^{-1}, while

Mg-O vibrational modes give rise to bands below 560 cm^{-1} [8]. A summary of these findings is depicted in Fig. 9.

3.5. Chemical element mapping

To validate the variations in the chemical composition on the Mg surface treated with different solutions, before the removal of degradation product, chemical element mapping was conducted for samples immersed in different media after different incubation time. The distributions of elements, carbon (C), oxygen (O), phosphorous (P), magnesium (Mg) and calcium (Ca) were probed for all samples after immersion (Ca only existed on the degradation layer formed in the media with FBS). The detected amount of S, Na and Cl was negligible for all samples (< 0.5 *wt.* %), hence the corresponding mappings are not presented in Fig. 7.

To highlight the most important points, element mappings of the degradation layers with different morphologies were selected to present the results of this measurement (Fig. 7). As expected, the existence of C, O, Mg in degradation layer tended to support that carbonate was one of the degradation products as revealed by both XRD and IR reflection spectra. Due to the similarity of the compositions between the "outer" precipitates and the "inner" degradation layer, it was hard to distinguish the boundary between these two layers. However, there was an obvious difference for the distributions of P in degradation products near Mg matrix. The existence of P indicated the formation of phosphate in the degradation layer. For the samples incubated in media with FBS, a thin P/Ca-rich layer formed after 3 days of incubation, indicating the formation of a more compact layer for Mg against the attack of aggressive ions in media [45]. The distribution of Ca was in accordance with that of P for the samples immersed in media with FBS, indicating the formation of Ca-P salts.

The weight percentage of P in the degradation products near Mg matrix was analyzed according to the chemical mapping to get the quantitative difference of the chemical compositions of degradation

layer. As shown in Fig. 8, after the addition of organic components, the contents of P in the degradation products significantly increased, especially for media with more than one kind of organic components. Moreover, the values also rose with immersion time. However, it should be noted that the content of P is quite low (< 6 *wt. %*) in the degradation products.

4. Discussion

In general, when Mg is immersed into aqueous solution, Mg dissolves into solution as Mg^{2+} and hydrogen is evolved by the following reactions [22].

$$Mg + 2H_2O \rightarrow Mg^{2+} + 2OH^- + H_2\uparrow \quad (2)$$

Along with the dissolution of Mg, the pH of the solution and the concentration of Mg^{2+} near the surface increase, resulting in the formation of degradation products on the surface. The critical Mg^{2+} concentrations for different products have been discussed in literature [30]. Therefore, several components as degradation products form on the surface according to the compositions of HBSS: $Mg(OH)_2$, $MgCO_3$ and $Mg_3(PO_4)_2$ [13, 30, 44].

$$Mg^{2+} + 2\ OH^- \rightarrow Mg(OH)_2 \quad (3)$$

$$Mg^{2+} + CO_3^{2-} \rightarrow MgCO_3 \quad (4)$$

$$3\ Mg^{2+} + 2\ PO_4^{3-} \rightarrow Mg_3(PO_4)_2 \quad (5)$$

$$x\ Mg^{2+} + y\ Ca^{2+} + z\ PO_4^{3-} \rightarrow Mg_xCa_y(PO_4)_z \quad (6)$$

The formation of Ca-P salts is also possible as shown in equation (6) when FBS is present due to the existence of Ca in FBS. In our study, the addition of the organic molecules leads to a high content of phosphorous in degradation products (Fig. 8), suggesting the organic molecules promote the formation of phosphates in the "inner" degradation layer which may inhibit the degradation of Mg.

Moreover, due to a more complex structure of protein, a P/Ca-rich layer forms on the sample surface in media with FBS (Fig. 7). It has been reported that some amino-functionalized materials were chosen as phosphate adsorbents to remove phosphate from aqueous solutions by electrostatic attraction and the adsorption capacity was almost unaffected by the presence of competitive ions but changed with pH and temperature [46-50]. Moreover, it has been found that the absorbed amino acids on surfaces can promote hydroxyapatite mineralization by attracting Ca^{2+} and PO_4^{3-} and increasing the local supersaturation [51]. These are possible explanations for the increased content of phosphate in the "inner" degradation layer formed in media with organics. However, the interaction between organic components and PO_4^{3-}/Ca^{2+}/Mg^{2+} still needs further investigation to elucidate the role of organic molecules in phosphate precipitation.

The continuous degradation of Mg leads to the increase of Mg^{2+} concentration and pH in media, eventually resulting in the saturation of Mg^{2+} for different salts (nesquehonite, hydromagnesite). Therefore, some precipiates also deposit on the surface from the solution to form the "outer" white, loosely bound precipitates layer. In our study, two different precipitates formed dominatly on the surface, hydromagnesite ($Mg_5(CO_3)_4(OH)_2\ 4H_2O$) and nesquehonite ($MgCO_3\ 3H_2O$) as shown in Fig. 5. Nesquehonite may be formed in three ways, directly precipitated from solution, hydrated from magnesite or transformed from hydromagnesite when the CO_2 pressure becomes sufficiently high [42, 52].

$$Mg^{2+} + CO_3^{2-} + 3H_2O \rightarrow MgCO_3\ 3H_2O \quad (7)$$

$$MgCO_3 + 3\ H_2O \rightarrow MgCO_3\ 3H_2O \quad (8)$$

$$Mg_5(CO_3)_4(OH)_2\ 4H_2O + CO_2 + 10\ H_2O \rightarrow 5\ MgCO_3\ 3H_2O \quad (9)$$

However, a number of possible ways also have been reported for the formation of hydromagnesite, for example, directly precipitated from solution. At high CO_2 pressure (about 10^{-5}-10^{-1} atm), magnesite can be hydrated to hydromagnesite along with the increase of water vapour pressure [42]. At high water vapour pressure (about $10^{-2.8}$~$10^{-1.5}$ atm), increasing CO_2 presure can convert magnesium hydroxide into hydromagnesite [42]. Hydromagnesite can also be formed by dehydration of nesquehonite [42].

$$5\ Mg^{2+} + 5\ OH^- + 4\ CO_3^{2-} + 4\ H_2O \rightarrow Mg_5(CO_3)_4(OH)_2\ 4H_2O \quad (10)$$

$$5\ MgCO_3 + 5H_2O \rightarrow Mg_5(CO_3)_4(OH)_2\ 4H_2O + CO_2 \quad (11)$$

$$5\ Mg(OH)_2 + 4\ CO_2 \rightarrow Mg_5(CO_3)_4(OH)_2\ 4H_2O \quad (12)$$

$$5\ MgCO_3\ 3H_2O \rightarrow Mg_5(CO_3)_4(OH)_2\ 4H_2O + CO_2 + 10\ H_2O \quad (13)$$

Based on the conditions used, the precipitates are possible formed by the equation (7, 8, 10, 11). The type of the "outer" precipitates (nesquehonite or hydromageniste) may affect the thickness of degradation layer. When nesqueshonite deposits on the surface, the degradation layer is significantly thinner than that with hydromagnesite precipitates (Fig.2c).

Under the conditions used in this study, hydromagensite forms on Mg surface in HBSS or HBSS with single organic component, while the addition of two or more kinds of organic components to HBSS leads to the formation of nesquehonite. There are two important factors for the formation of different precipitates on Mg surface: pH and free Mg^{2+} concentration. The changes in pH do not only depend on the buffering of HCO_3^-/CO_2. The addition of organic components, especially when at least two kinds of organic components were added, results in a lower pH than in HBSS during the immersion. This may be related to the buffering capacity of the carboxyl-groups and amino-groups, since the pH values were still lower than that of HBSS even after 14 days' incubation when the

degradation rates of samples in the organic-containing media were already higher than that of the control (Fig. 1). On the other hand, the obvious feature for the media containing the organic components is the higher osmolality compared with that in HBSS solution (Fig.2b). The osmolality is mainly attributed to the Mg^{2+} of the solution. It can be explained by the binding of ions to the organic molecules presented and the chelating effect of amino acids and proteins [28, 53-55]. The binding and chelating of proteins have already been proven [56-58], which can lead to the higher osmolality of media. The formation of different precipitates on Mg surface in HBSS-based media indicates a stronger regulating ability of the mixture of the organic components for pH and free Mg^{2+} concentration than single organic components, resulting in the faster degradation of Mg in HBSS with more organic components as shown in Fig. 1. This interaction between various factors is difficult to display or examine in simplified experiments, however, we believe that the application of physiological conditions is an important factor for experimental setups.

The decrease of L-Gln concentration after 20 hours immersion (Fig. 3b) indicates the participation of L-Gln in the degradation process by adsorption or other ways. L-AA and Amino acids have already been evaluated as corrosion inhibitor for Mg alloys, Al alloys or steel due to their adsorption on sample surface [59-63]. The corrosion inhibition of BSA has also been studied and is due to the physical/chemical adsorption or the chemical binding of protein to magnesium on the surface [19, 64]. Furthermore, proteins can adsorb on the degradation products by tightly binding to oxygen atoms through acid/base interactions [65]. These results on the adsorption of organic molecules are in agreement with the decrease of L-Gln concentration (Fig. 3). Moreover, the adsorption of organic melocules can also affect the growth direction of crystals [66], thereby affecting the morphology of precipitates on the surface. This is one of possible reasons for the change of the morphology of nesquehonite when FBS is present in media.

During the immersion test, the media were changed every 2 or 3 days to present a semi-static condition, which results in fresh media with low osmolality and low pH after the change of media. This condition lead to the dissolution or transformation of nesquehonite, resulting in the change of morphology with immersion time (Fig. 4b), because the solubility and stability of nesquehonite is related to the concentration of Mg^{2+} and pH [67, 68]. It has also been demonstrated that nesquehonite, as the precursor of hydromagnesite, can decompose to hydromagnesite with the formation of some intermediate hydrate phases, such as, dypingite and protohydromagnesite. [52, 69]. The transformation between these carbonates is tightly related to the fluctuation of some parameters, eg. pH，Mg^{2+} concentration, temperature, etc. [70]. The processes of precipitation are quite complex, since the family of magnesium carbonates consists of a variety of compounds and they can be transformed into each other under certain conditions [69, 71, 72]. Therefore, a slight change of parameters in the immersion experiment setups in other studies might lead to the formation of other members of this family. These basic mechanisms are depicted in Fig. 9.

Concerning the effect of organic molecules on degradation rate of Mg, the previous investigations draw different conclusions for the effect of small organic molecules on Mg degradation. Wang et al. indicated that L-cysteine (6 mg/L) would inhibit the corrosion of pure Mg in 0.9 wt. % NaCl solution due to the adsorption on Mg surface [73]. However, under cell culture conditions, the mixture of more organic components (amino acids, vitamins) would promote the release of Mg ion to E-MEM and increase the degradation rate of pure Mg from 0.468 mm/year to 0.676 mm/year after 14 days of immersion in MEM [15, 22], which is consistent with our result that organic components increase the degradtaion of Mg after 14 days of immersion. Our results showed that the mixture of organic molecules gives stronger influence for Mg degrataion than the single organic molecule. Therefore,

these different conclusions or uncomparable degradation rates from these investigations may ascribe to different content or kinds of organic molecules used and different base medium used.

Similar results can be assumed for pure Mg in DMEM that the presence of amino acids and vitamins in DMEM also could affect the degradation of Mg under cell culture conditions [20]. DMEM commonly was used to evaluate the degradation of Mg *in vitro* due to a comparable degradation rate and degradation layer in DMEM to *in vivo* conditions [6]. Moreover, DMEM also contains abundant small organic molecules, such as, amino acids, vitamins. The precipitate (nesquehonite) also was found to form on Mg surface in DMEM [28, 30], as formed in HBSS with the mixture of organic molecules. Generally, the degradation rate of pure Mg is around or below 1 mm/year in DMEM [5, 6], which is lower than in HBSS-based media (1-3 mm/year in this study). This slower degradation of Mg in DMEM mainly results from Ca^{2+} and high concentration of HCO_3^- [13]. Furthermore, the degradation rate of pure Mg *in vivo* is normally below 1 mm/year and the degradation layer formed on Mg surface always is found to be two layer: inner layer and outer P/Ca layer, and the out P/Ca layer is believed to deposit on sample surface during implantation [5, 6, 15, 74]. However, the outer precipitate layers are formed by crystalline carbonates in this study. This difference is due to the shortage of Ca/Mg ions, organic components in media, and the absence of cells in this study compared with *in vivo* conditions. Although the degradation rate and degradation products is not completely comparable to *in vivo* conditions, our approach can still give some information about the role of organic molecules in the degradation of Mg.

In summary, our study shows that organic molecules do not significantly affect the degradation rate of pure Mg during a relatively short-term immersion, but after a long-term exposure they encourage the dissolution of Mg. More important, the organic components play an important role in the formation of degradation products, which largely affect the formation of precipitates in the “outer”

layer and evidently promote the formation of phosphate in the "inner" layer. The promotion of phosphate formation in organic-containing media may be related to the surface biomineralization and tissue regeneration during *in vivo* tests [75]. These results indicate that the addition of organic components not only supports cell proliferation or tissue culture, but also changes the surface conditions (surface product, charge, roughness, etc.) of Mg for cell adhesion or biological performance of materials. Moreover, during *in vivo* investigations, the cells or tissues can release some organic molecules during the interaction with materials after implantation, for example, the adhesion of osteoblasts is achieved via the adhesive proteins [76]. These organic molecules also can affect the degradation of Mg implants. Although the conditions used in this study are still different to *in vivo* conditions, it can provide some references for the understanding on the *in vivo* degradation of Mg when organic components are present. A further more physiological conditions (complex medium, flow conditions, etc.) and more detailed investigations on the influence of organic components are still needed to achieve a clear understanding on the *in vivo* degradation of Mg.

5. Conclusions

We have first insights into the interplay between organic components and Mg degradation under physiological conditions. Unexpectedly, the influence of organic components on the degradation rate and layer composition was time-dependent. Although the conditions used in this study is still far away from the *in vivo* conditions, a fundamental conclusion can be draw that the presence of organic molecules in test medium plays an important role in the formation of degradation products, suggesting the different compositions of degradation products between *in vitro* and *in vivo* investigations. In other words, the organic components not only affect the degradation rate of Mg, but also result in a different degradation surface for cells or tissues during *in vitro* tests, then leading

to a possible different degradation and biological performance of materials. Moreover, the promotion of phosphate in degradation layer by organic components suggests the interaction between organic components and surface biomineralization or tissue regeneration. Therefore, we recommend the addition of organic components to test medium for *in vitro* Mg characterization to obtain reliable results compared with *in vivo* tests.

Acknowledgements

We would like to thank the China Scholarship Council (CSC) for a scholarship to the first author. The research leading to these results has received funding from the Helmholtz Virtual Institute "In vivo studies of biodegradable magnesium based implant materials (MetBioMat)" (grant number: VH-VI-523). Sincerest gratitude goes to the colleagues from the Division of Metallic Biomaterials (HZG) for their invaluable technical supports and discussions.

References

[1] Y. Chen, Z. Xu, C. Smith, J. Sankar, Recent advances on the development of magnesium alloys for biodegradable implants, Acta Biomater., 10 (2014) 4561-4573.

[2] S. Agarwal, J. Curtin, B. Duffy, S. Jaiswal, Biodegradable magnesium alloys for orthopaedic applications: A review on corrosion, biocompatibility and surface modifications, Mat. Sci. Eng. C-Mater. Biol. Appl., 68 (2016) 948-963.

[3] Y.-L. Zhou, Y. Li, D.-M. Luo, Y. Ding, Influence of extrusion on the microstructure, mechanical properties and in vitro corrosion performance of biodegradable Mg-1Mn-2Zn-1Nd alloy, Mater. Technol., (2016) 1-5.

[4] D. Zhao, F. Witte, F. Lu, J. Wang, J. Li, L. Qin, Current status on clinical applications of magnesium-based orthopaedic implants: A review from clinical translational perspective, Biomaterials, 112 (2017) 287-302.

[5] A. Myrissa, N.A. Agha, Y. Lu, E. Martinelli, J. Eichler, G. Szakács, C. Kleinhans, R. Willumeit-Römer, U. Schäfer, A.-M. Weinberg, In vitro and in vivo comparison of binary Mg alloys and pure Mg, Mat. Sci. Eng. C-Mater. Biol. Appl., 61 (2016) 865-874.

[6] I. Marco, A. Myrissa, E. Martinelli, F. Feyerabend, R. Willumeit-Römer, A. Weinberg, O. Van der Biest, In vivo and in vitro degradation comparison of pure Mg, Mg-10Gd and Mg-2Ag: a short term study, Eur. Cells Mater., 33 (2017) 90-104.

[7] F. Witte, V. Kaese, H. Haferkamp, E. Switzer, A. Meyer-Lindenberg, C. Wirth, H. Windhagen, In vivo corrosion of four magnesium alloys and the associated bone response, Biomaterials, 26 (2005) 3557-3563.

[8] Y. Xin, K. Huo, H. Tao, G. Tang, P.K. Chu, Influence of aggressive ions on the degradation behavior of biomedical magnesium alloy in physiological environment, Acta Biomater., 4 (2008) 2008-2015.

[9] Z. Li, G.-L. Song, S. Song, Effect of bicarbonate on biodegradation behaviour of pure magnesium in a simulated body fluid, Electrochim. Acta, 115 (2014) 56-65.

[10] C. Taltavull, Z. Shi, B. Torres, J. Rams, A. Atrens, Influence of the chloride ion concentration on the corrosion of high-purity Mg, ZE41 and AZ91 in buffered Hank's solution, J. Mater. Sci. M., 25 (2014) 329-345.

[11] S. Johnston, Z. Shi, A. Atrens, The influence of pH on the corrosion rate of high-purity Mg, AZ91 and ZE41 in bicarbonate buffered Hanks' solution, Corros. Sci., 101 (2015) 182-192.

[12] C. Ning, L. Zhou, Y. Zhu, Y. Li, P. Yu, S. Wang, T. He, W. Li, G. Tan, Y. Wang, Influence of Surrounding Cations on the Surface Degradation of Magnesium Alloy Implants under a Compressive Pressure, Langmuir., 31 (2015) 13561-13570

[13] N.A. Agha, F. Feyerabend, B. Mihailova, S. Heidrich, U. Bismayer, R. Willumeit-Romer, Magnesium degradation influenced by buffering salts in concentrations typical of in vitro and in vivo models, Mater. Sci. Eng. C-Mater. Biol. Appl., 58 (2016) 817-825.

[14] D. Höche, C. Blawert, S.V. Lamaka, N. Scharnagl, C. Mendis, M.L. Zheludkevich, The effect of iron re-deposition on the corrosion of impurity-containing magnesium, Phys. Chem. Chem. Phys., 18 (2016) 1279-1291.

[15] J. Walker, S. Shadanbaz, N.T. Kirkland, E. Stace, T. Woodfield, M.P. Staiger, G.J. Dias, Magnesium alloys: predicting in vivo corrosion with in vitro immersion testing, J Biomed Mater Res B Appl Biomater, 100 (2012) 1134-1141.

[16] M.-C. Zhao, M. Liu, G.-L. Song, A. Atrens, Influence of pH and chloride ion concentration on the corrosion of Mg alloy ZE41, Corros. Sci., 50 (2008) 3168-3178.

[17] F. Witte, J. Fischer, J. Nellesen, H.-A. Crostack, V. Kaese, A. Pisch, F. Beckmann, H. Windhagen, In vitro and in vivo corrosion measurements of magnesium alloys, Biomaterials, 27 (2006) 1013-1018.

[18] A.H. Martinez Sanchez, B.J. Luthringer, F. Feyerabend, R. Willumeit, Mg and Mg alloys: how comparable are in vitro and in vivo corrosion rates? A review, Acta Biomater., 13 (2015) 16-31.

[19] C. Liu, Y. Xin, X. Tian, P.K. Chu, Degradation susceptibility of surgical magnesium alloy in artificial biological fluid containing albumin, J. Mater. Res., 22 (2007) 1806-1814.

[20] X. Gu, Y. Zheng, L. Chen, Influence of artificial biological fluid composition on the biocorrosion of potential orthopedic Mg–Ca, AZ31, AZ91 alloys, Biomed. Mater., 4 (2009) 065011.
[21] W.D. Mueller, M. Fernández Lorenzo de Mele, M.L. Nascimento, M. Zeddies, Degradation of magnesium and its alloys: dependence on the composition of the synthetic biological media, J. Biomed. Mater. Res. A, 90 (2009) 487-495.
[22] A. Yamamoto, S. Hiromoto, Effect of inorganic salts, amino acids and proteins on the degradation of pure magnesium in vitro, Mat. Sci. Eng. C-Mater. Biol. Appl., 29 (2009) 1559-1568.
[23] Y. Wang, C.S. Lim, C.V. Lim, M.S. Yong, E.K. Teo, L.N. Moh, In vitro degradation behavior of M1A magnesium alloy in protein-containing simulated body fluid, Mat. Sci. Eng. C-Mater. Biol. Appl., 31 (2011) 579-587.
[24] M.S. Killian, V. Wagener, P. Schmuki, S. Virtanen, Functionalization of metallic magnesium with protein layers via linker molecules, Langmuir., 26 (2010) 12044-12048.
[25] P.-L. Jiang, R.-Q. Hou, C.-D. Chen, L. Sun, S.-G. Dong, J.-S. Pan, C.-J. Lin, Controllable Degradation of Medical Magnesium by Electrodeposited Composite Films of Mussel Adhesive Protein (Mefp-1) and Chitosan, J. Colloid Interf. Sci, 478 (2016) 246–255.
[26] R.-Q. Hou, P.-L. Jiang, S.-G. Dong, C.-J. Lin, NaIO4 Oxidation of Mussel Adhesive Protein Film and Its Corrosion Protection for Mg-1.0Ca Alloy, J. Electrochem., 21 (2015) 58-65.
[27] V. Wagener, S. Virtanen, Protective layer formation on magnesium in cell culture medium, Mat. Sci. Eng. C-Mater. Biol. Appl., 63 (2016) 341-351.
[28] R. Willumeit, J. Fischer, F. Feyerabend, N. Hort, U. Bismayer, S. Heidrich, B. Mihailova, Chemical surface alteration of biodegradable magnesium exposed to corrosion media, Acta Biomater., 7 (2011) 2704-2715.
[29] R. Harrison, D. Maradze, S. Lyons, Y.F. Zheng, Y. Liu, Corrosion of magnesium and magnesium-calcium alloy in biologically-simulated environment, Prog. Nat. Sci.-Mater., 24 (2014) 539-546.
[30] M. Kieke, F. Feyerabend, J. Lemaitre, P. Behrens, R. Willumeit-Römer, Degradation rates and products of pure magnesium exposed to different aqueous media under physiological conditions, BioNanoMaterials, 17 (2016) 131-143.
[31] A. Diplock, J.-L. Charuleux, G. Crozier-Willi, F. Kok, C. Rice-Evans, M. Roberfroid, W. Stahl, J. Vina-Ribes, Functional food science and defence against reactive oxidative species, Brit. J. Nutr., 80 (1998) S77-S112.
[32] M.W. Davey, M.v. Montagu, D. Inzé, M. Sanmartin, A. Kanellis, N. Smirnoff, I.J.J. Benzie, J.J. Strain, D. Favell, J. Fletcher, Plant L‐ascorbic acid: chemistry, function, metabolism, bioavailability and effects of processing, J. Sci. Food Agr., 80 (2000) 825-860.
[33] P. Felig, Amino acid metabolism in man, Annu. Rev. Biochem., 44 (1975) 933-955.
[34] P.A. MacLennan, R. Brown, M.J. Rennie, A positive relationship between protein synthetic rate and intracellular glutamine concentration in perfused rat skeletal muscle, Febs. Lett., 215 (1987) 187-191.
[35] M. Jepson, P. Bates, P. Broadbent, J. Pell, D. Millward, Relationship between glutamine concentration and protein synthesis in rat skeletal muscle, Am. J. Physiol-endoc. M, 255 (1988) E166-E172.
[36] P. Newsholme, J. Procopio, M.M.R. Lima, T.C. Pithon‐Curi, R. Curi, Glutamine and glutamate—their central role in cell metabolism and function, Cell Biochem. Funct., 21 (2003) 1-9.
[37] R. Curi, C.J. Lagranha, D. Sellitti, J. Procopio, T. Pithon‐Curi, M. Corless, P. Newsholme, Molecular mechanisms of glutamine action, J. Cell Physiol., 204 (2005) 392-401.
[38] E.P. Rutten, M.P. Engelen, A.M. Schols, N.E. Deutz, Skeletal muscle glutamate metabolism in health and disease: state of the art, Curr. Opin. Clin. Nutr., 8 (2005) 41-51.
[39] P. Fürst, P. Stehle, What are the essential elements needed for the determination of amino acid requirements in humans?, J. Nutr., 134 (2004) 1558S-1565S.
[40] R.C. Harris, J.R. Hoffman, A. Allsopp, N.B. Routledge, L-glutamine absorption is enhanced after ingestion of L-alanylglutamine compared with the free amino acid or wheat protein, Nutr. Res., 32 (2012) 272-277.
[41] E.P.S. Nidadavolu, F. Feyerabend, T. Ebel, R. Willumeit-Römer, M. Dahms, On the Determination of Magnesium Degradation Rates under Physiological Conditions, Materials, 9 (2016) 627-637.

[42] M. Jönsson, D. Persson, D. Thierry, Corrosion product formation during NaCl induced atmospheric corrosion of magnesium alloy AZ91D, Corros. Sci., 49 (2007) 1540-1558.
[43] Y. Yu, X. Fei, J. Tian, L. Xu, X. Wang, Y. Wang, Self-assembled enzyme–inorganic hybrid nanoflowers and their application to enzyme purification, Colloids and Surfaces B: Biointerfaces, 130 (2015) 299-304.
[44] D. Tie, F. Feyerabend, N. Hort, R. Willumeit, D. Hoeche, XPS studies of magnesium surfaces after exposure to Dulbecco's Modified Eagle Medium, Hank's buffered salt solution, and simulated body fluid, Adv. Eng. Mater., 12 (2010) B699-B704.
[45] Y. Jang, B. Collins, J. Sankar, Y. Yun, Effect of biologically relevant ions on the corrosion products formed on alloy AZ31B: an improved understanding of magnesium corrosion, Acta Biomater., 9 (2013) 8761-8770.
[46] R. Saad, K. Belkacemi, S. Hamoudi, Adsorption of phosphate and nitrate anions on ammonium-functionalized MCM-48: Effects of experimental conditions, J. Colloid Interf. Sci, 311 (2007) 375-381.
[47] H.Y. Shen, Z.J. Wang, A. Zhou, J.L. Chen, M.Q. Hu, X.Y. Dong, Q.H. Xia, Adsorption of phosphate onto amine functionalized nano-sized magnetic polymer adsorbents: mechanism and magnetic effects, RSC Adv., 5 (2015) 22080-22090.
[48] Y. Zhang, X. Xi, S. Xu, J. Zhou, J. Zhou, Q. Xu, H. Shen, Adsorption studies on phosphate by amino-functionalized nano-size composite materials, Acta Chim. Sinica., 70 (2012) 1839-1846.
[49] J.K. Kang, J.H. Kim, S.B. Kim, S.H. Lee, J.W. Choi, C.G. Lee, Ammonium-functionalized mesoporous silica MCM-41 for phosphate removal from aqueous solutions, Desalin. Water Treat., 57 (2016) 10839-10849.
[50] Z.F. Ren, X. Xu, X. Wang, B.Y. Gao, Q.Y. Yue, W. Song, L. Zhang, H.T. Wang, FTIR, Raman, and XPS analysis during phosphate, nitrate and Cr(VI) removal by amine cross-linking biosorbent, J. Colloid Interf. Sci, 468 (2016) 313-323.
[51] M. Tavafoghi, M. Cerruti, The role of amino acids in hydroxyapatite mineralization, J. R. Soc. Interface, 13 (2016) 20160462.
[52] J.T. Kloprogge, W.N. Martens, L. Nothdurft, L.V. Duong, G.E. Webb, Low temperature synthesis and characterization of nesquehonite, J. Mater. Sci. Lett., 22 (2003) 825-829.
[53] R.E. Cian, A.G. Garzón, D.B. Ancona, L.C. Guerrero, S.R. Drago, Chelating Properties of Peptides from Red Seaweed Pyropia columbina and Its Effect on Iron Bio-Accessibility, Plant Food Hum. Nutr., 71 (2016) 96-101.
[54] C. Orme, A. Noy, A. Wierzbicki, M. McBride, M. Grantham, H. Teng, P. Dove, J. DeYoreo, Formation of chiral morphologies through selective binding of amino acids to calcite surface steps, Nature, 411 (2001) 775-779.
[55] M. Seddigh, A.H. Khoshgoftarmanesh, S. Ghasemi, The effectiveness of seed priming with synthetic zinc-amino acid chelates in comparison with soil-applied ZnSO4 in improving yield and zinc availability of wheat grain, J. Plant Nutr., 39 (2016) 417-427.
[56] T. Kosa, T. Maruyama, M. Otagiri, Species differences of serum albumins: I. Drug binding sites, Pharmaceut. Res., 14 (1997) 1607-1612.
[57] B.X. Huang, H.-Y. Kim, C. Dass, Probing three-dimensional structure of bovine serum albumin by chemical cross-linking and mass spectrometry, J. Am. Soc. Mass. Spectr, 15 (2004) 1237-1247.
[58] A. Michnik, K. Michalik, A. Kluczewska, Z. Drzazga, Comparative DSC study of human and bovine serum albumin, J. Therm. Anal. Calorim, 84 (2005) 113-117.
[59] H. Ashassi-Sorkhabi, M.R. Majidi, K. Seyyedi, Investigation of inhibition effect of some amino acids against steel corrosion in HCl solution, Appl. Surf. Sci., 225 (2004) 176-185.
[60] E. Ferreira, C. Giacomelli, F. Giacomelli, A. Spinelli, Evaluation of the inhibitor effect of L-ascorbic acid on the corrosion of mild steel, Mater. Chem. Phys., 83 (2004) 129-134.
[61] H. Ashassi-Sorkhabi, Z. Ghasemi, D. Seifzadeh, The inhibition effect of some amino acids towards the corrosion of aluminum in 1M HCl+1M H2SO4 solution, Appl. Surf. Sci., 249 (2005) 408-418.
[62] M.A. Amin, K.F. Khaled, Q. Mohsen, H.A. Arida, A study of the inhibition of iron corrosion in HCl solutions by some amino acids, Corros. Sci., 52 (2010) 1684-1695.
[63] N.H. Helal, W.A. Badawy, Environmentally safe corrosion inhibition of Mg–Al–Zn alloy in chloride free neutral solutions by amino acids, Electrochim. Acta, 56 (2011) 6581-6587.

[64] C.L. Liu, Y.J. Wang, R.C. Zeng, X.M. Zhang, W.J. Huang, P.K. Chu, In vitro corrosion degradation behaviour of Mg–Ca alloy in the presence of albumin, Corros. Sci., 52 (2010) 3341-3347.
[65] T.R. Cundari, A.K. Wilson, M.L. Drummond, H.E. Gonzalez, K.R. Jorgensen, S. Payne, J. Braunfeld, M. De Jesus, V.M. Johnson, CO2-formatics: how do proteins bind carbon dioxide?, J. Chem. Inf. Model., 49 (2009) 2111-2115.
[66] P.K. Yan, B. Wang, Y.J. Gao, Study on synthesis of the high aspect ratios nesquehonite whiskers, in: Adv. Mater. Res., Trans Tech Publ, 2011, pp. 1118-1122.
[67] M. Dong, W. Cheng, Z. Li, G.P. Demopoulos, Solubility and stability of nesquehonite (MgCO3 · 3H2O) in NaCl, KCl, MgCl2, and NH4Cl solutions, J. Chem. Eng. Data, 53 (2008) 2586-2593.
[68] M. Dong, Z. Li, J. Mi, G.P. Demopoulos, Solubility and stability of nesquehonite (MgCO3 · 3H2O) in mixed NaCl+ MgCl2, NH4Cl+ MgCl2, LiCl, and LiCl+ MgCl2 solutions, J. Chem. Eng. Data, 54 (2009) 3002-3007.
[69] P.J. Davies, B. Bubela, The transformation of nesquehonite into hydromagnesite, Chem. Geol., 12 (1973) 289-300.
[70] A.P.A. dos Anjos, A. Sifeddine, C.J. Sanders, S.R. Patchineelam, Synthesis of magnesite at low temperature, Carbonate. Evaporite., 26 (2011) 213-215.
[71] Z. Zhang, Y. Zheng, Y. Ni, Z. Liu, J. Chen, X. Liang, Temperature-and pH-dependent morphology and FT-IR analysis of magnesium carbonate hydrates, J. Phys. Chem. B, 110 (2006) 12969-12973.
[72] J. Canterford, G. Tsambourakis, B. Lambert, Some observations on the properties of dypingite, Mg5 (CO3) 4 (OH) 2 ·5H2O, and related minerals, Mineral. Mag., 48 (1984) 437-442.
[73] Y. Wang, L.-Y. Cui, R.-C. Zeng, S.-Q. Li, Y.-H. Zou, E.-H. Han, In Vitro Degradation of Pure Magnesium—The Effects of Glucose and/or Amino Acid, Materials, 10 (2017) 725-740.
[74] P.K. Bowen, J. Drelich, J. Goldman, Magnesium in the murine artery: Probing the products of corrosion, Acta Biomater., 10 (2014) 1475-1483.
[75] Q. YE, R. HU, J.-Z. ZHOU, Y.-W. YE, Z.-X. XU, C.-J. LIN, Z.-Y. LIN, FTIR-ATR Spectrometry of BSA Adsorption on Hydroxyapatite, Acta Phys. Chim. Sin., 32 (2016) 565-572.
[76] K. Anselme, Osteoblast adhesion on biomaterials, Biomaterials, 21 (2000) 667-681.

Figures

Fig. 1 Mean degradation depths of pure Mg after immersion for 3, 7 and 14 days in different media under cell culture conditions. (One-way ANOVA, Dunn's test, Significance level: (*): $p<0.05$, (**): $p<0.01$)

Fig. 2 Changes in pH (a) and osmolality (b) after different days of incubation under cell culture condition in different media, Box and Whisker plot of the layer thickness (c) after different incubation time in different media. (The boxes (bottom to top) show the 25th percentile, median and 75th percentile. The whiskers mark the 10th and 90th percentiles, the rectangular points in the box are average values, significance level: (*): $p<0.05$, (**): $p<0.01$)

Fig. 3 The changes of pH (a) and L-Gln concentration (b) during the immersion. The absence of data during the initial immersion resulted from the range of on-line pH device (measurement range: pH 5 - 9), when pH is higher than 9, it can not be detemined by the device. (The grey background indicates the stable pH)

Fig. 4 SEM images of samples immersed in different media for different time (the compositions of media are listed in the above table, + refers to the existence of the component in medium, - refers to the absence of the component in medium).

Fig.5 XRD patterns of samples with different morphologies before and after the removal of white precipitates ((1) refers to the surfaces in HBSS with two kinds of organic components, (2) refers to the surfaces in HBSS with three kinds of organic components, (3) refers to the surfaces in HBSS or HBSS with one kind of organic components).

Fig. 6 Typical IR reflection spectra of the "inner" degradation layers on Mg formed in different media. (Light grey region refers to the bands from carbonate or organic components, Dark grey region refers to the bands from phosphate)

Fig. 7 BSE images and chemical element mappings of Mg samples exposed to HBSS with different organic components for different days.

Fig. 8 The weight percentages of P in degradation products near the Mg matrix in different media.

Fig. 9 Schematic illustration of degradation of pure Mg in different media. (a) pure Mg; (b)-(d) degradation in (I) HBSS or HBSS with one kind of organic components; (e)-(f) degradation in (II) HBSS with two kinds of organic components; (h)-(j) degradation in (III) HBSS with three kinds of organic components. The conditions for (b-j) are cell culture conditions as indicated in (a). The deeper color of media indicates the larger osmolality of media, the deeper color of "inner" layer indicates the higher content of phosphate.

Fig. 1

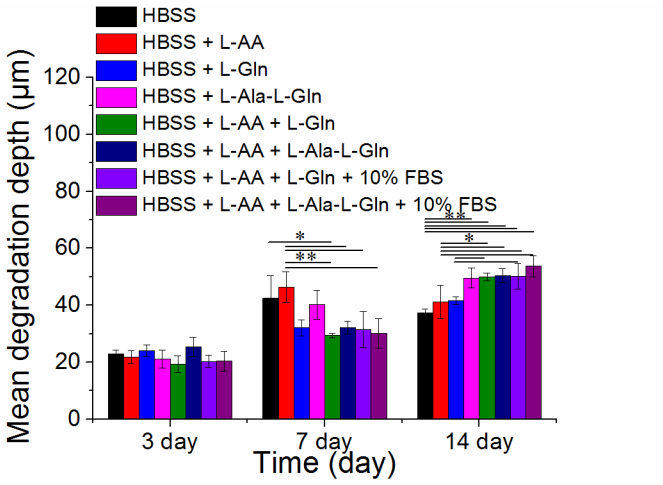
HBSS
HBSS + L-AA
HBSS + L-Gln
HBSS + L-Ala-L-Gln
HBSS + L-AA + L-Gln
HBSS + L-AA + L-Ala-L-Gln
HBSS + L-AA + L-Gln + 10% FBS
HBSS + L-AA + L-Ala-L-Gln + 10% FBS
Mean degradation depth (μm)
0
20
40
60
80
100
120
3 day
7 day
14 day
Time (day)
*
**
**
*
*

Fig. 2

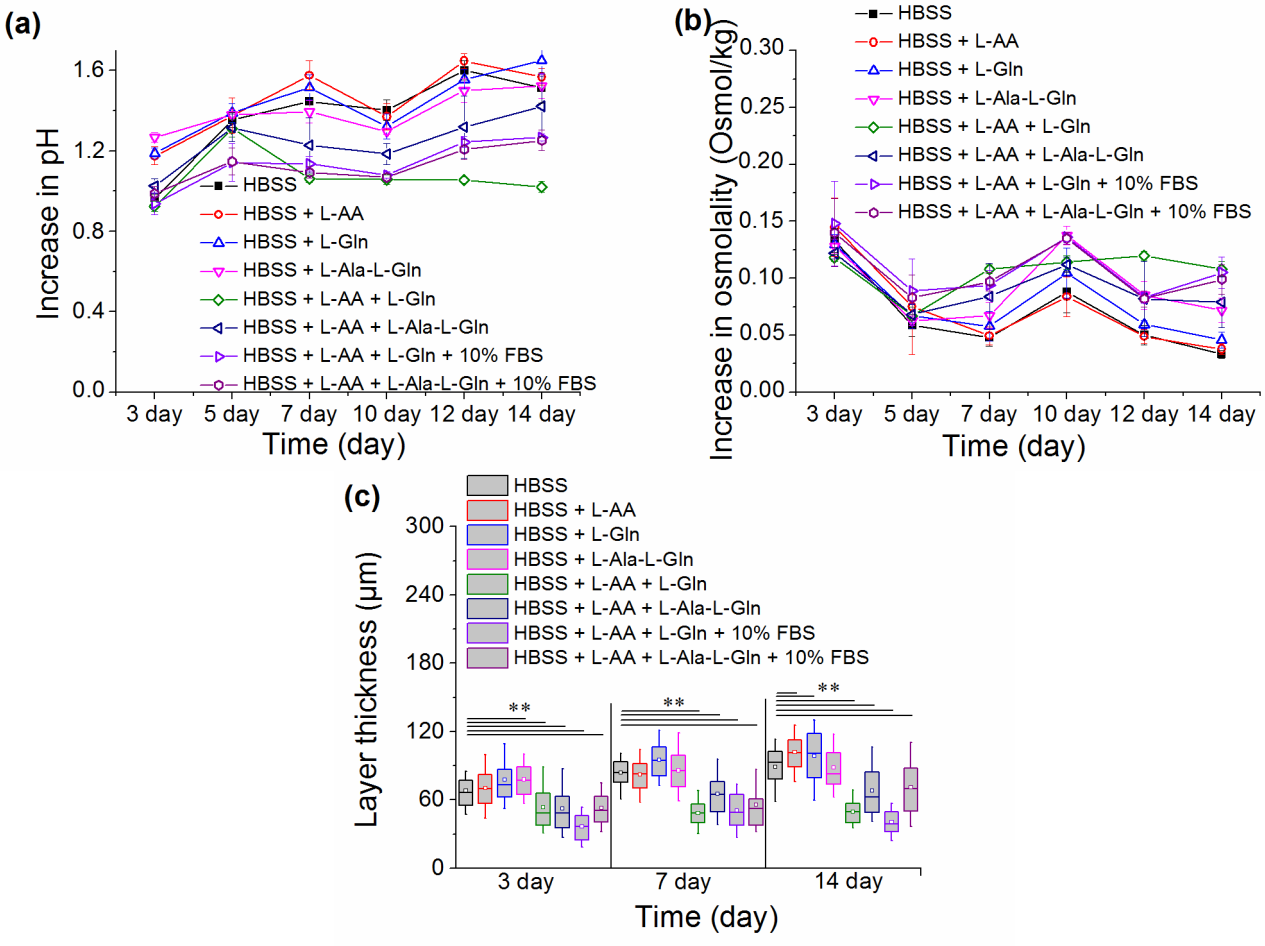
(a)
Increase in pH
0.0
0.4
0.8
1.2
1.6
3 day
5 day
7 day
10 day
12 day
14 day
Time (day)
HBSS
HBSS + L-AA
HBSS + L-Gln
HBSS + L-Ala-L-Gln
HBSS + L-AA + L-Gln
HBSS + L-AA + L-Ala-L-Gln
HBSS + L-AA + L-Gln + 10% FBS
HBSS + L-AA + L-Ala-L-Gln + 10% FBS
(b)
Increase in osmolality (Osmol/kg)
0.00
0.05
0.10
0.15
0.20
0.25
0.30
3 day
5 day
7 day
10 day
12 day
14 day
Time (day)
HBSS
HBSS + L-AA
HBSS + L-Gln
HBSS + L-Ala-L-Gln
HBSS + L-AA + L-Gln
HBSS + L-AA + L-Ala-L-Gln
HBSS + L-AA + L-Gln + 10% FBS
HBSS + L-AA + L-Ala-L-Gln + 10% FBS
(c)
Layer thickness (μm)
0
60
120
180
240
300
3 day
7 day
14 day
Time (day)
HBSS
HBSS + L-AA
HBSS + L-Gln
HBSS + L-Ala-L-Gln
HBSS + L-AA + L-Gln
HBSS + L-AA + L-Ala-L-Gln
HBSS + L-AA + L-Gln + 10% FBS
HBSS + L-AA + L-Ala-L-Gln + 10% FBS
**
**
**

Fig. 3

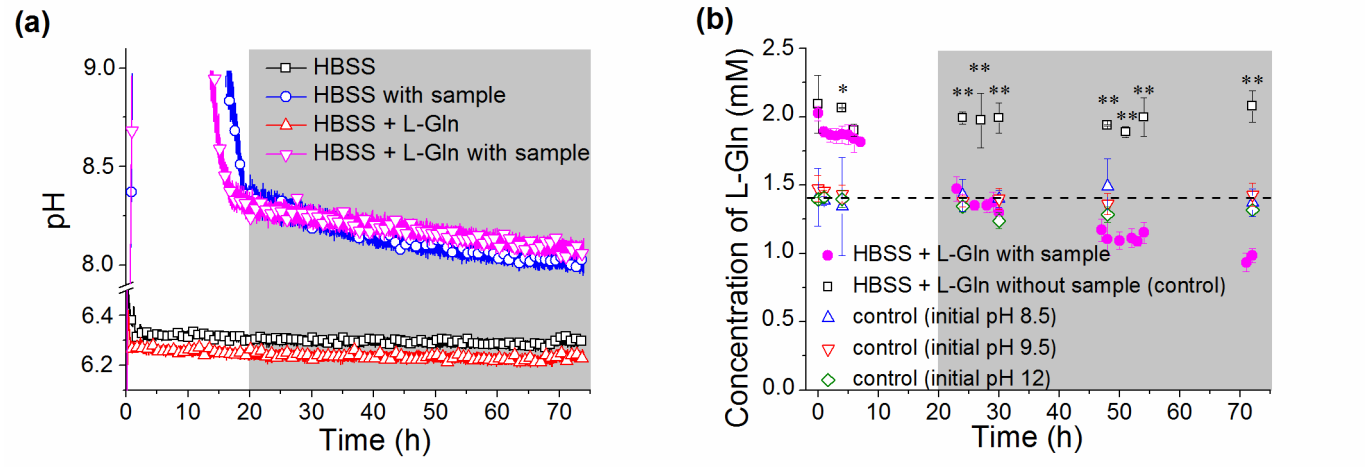
(a)
pH
Time (h)
HBSS
HBSS with sample
HBSS + L-Gln
HBSS + L-Gln with sample
(b)
Concentration of L-Gln (mM)
Time (h)
HBSS + L-Gln with sample
HBSS + L-Gln without sample (control)
control (initial pH 8.5)
control (initial pH 9.5)
control (initial pH 12)

Fig. 4

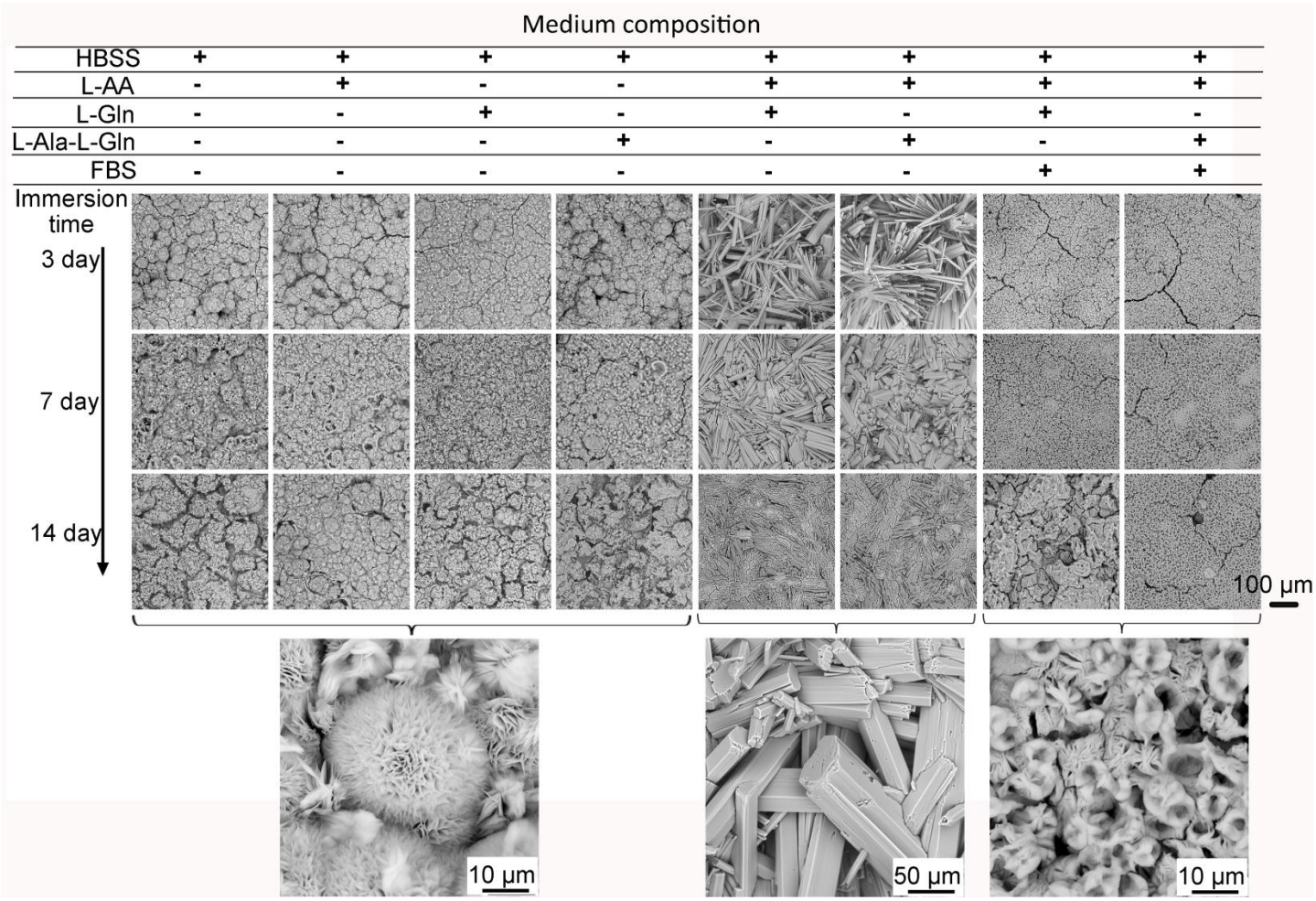
Medium composition
HBSS + + + + + + + +
L-AA - + - - + + + +
L-Gln - - + - + - + -
L-Ala-L-Gln - - - + - + - +
FBS - - - - - - + +
Immersion time
3 day
7 day
14 day
100 μm
10 μm
50 μm
10 μm

Fig. 5

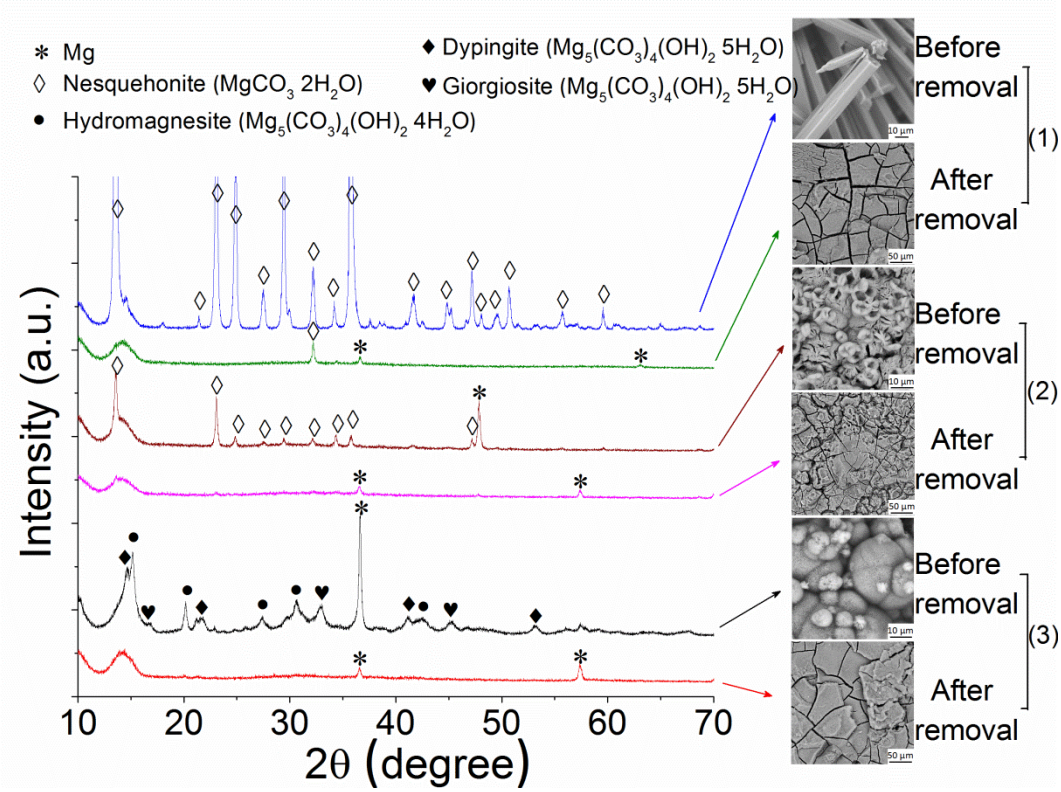
* Mg
◊ Nesquehonite (MgCO3 2H2O)
• Hydromagnesite (Mg5(CO3)4(OH)2 4H2O)
♦ Dypingite (Mg5(CO3)4(OH)2 5H2O)
♥ Giorgiosite (Mg5(CO3)4(OH)2 5H2O)
Intensity (a.u.)
2θ (degree)
10
20
30
40
50
60
70
Before removal
After removal
(1)
Before removal
After removal
(2)
Before removal
After removal
(3)

Fig. 6

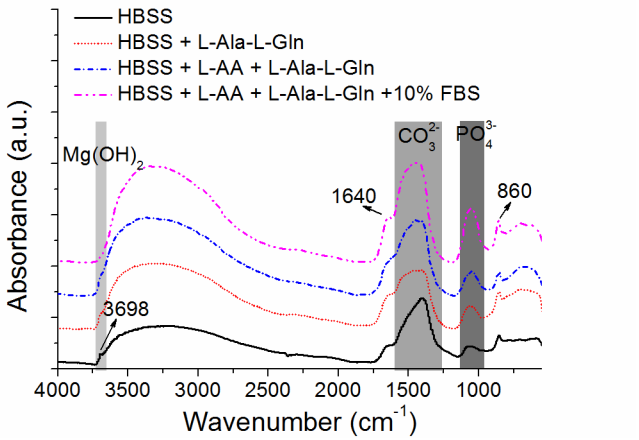
HBSS
HBSS + L-Ala-L-Gln
HBSS + L-AA + L-Ala-L-Gln
HBSS + L-AA + L-Ala-L-Gln +10% FBS
Mg(OH)2
CO3 2-
PO4 3-
1640
860
3698
Absorbance (a.u.)
4000
3500
3000
2500
2000
1500
1000
Wavenumber (cm-1)

Fig. 7

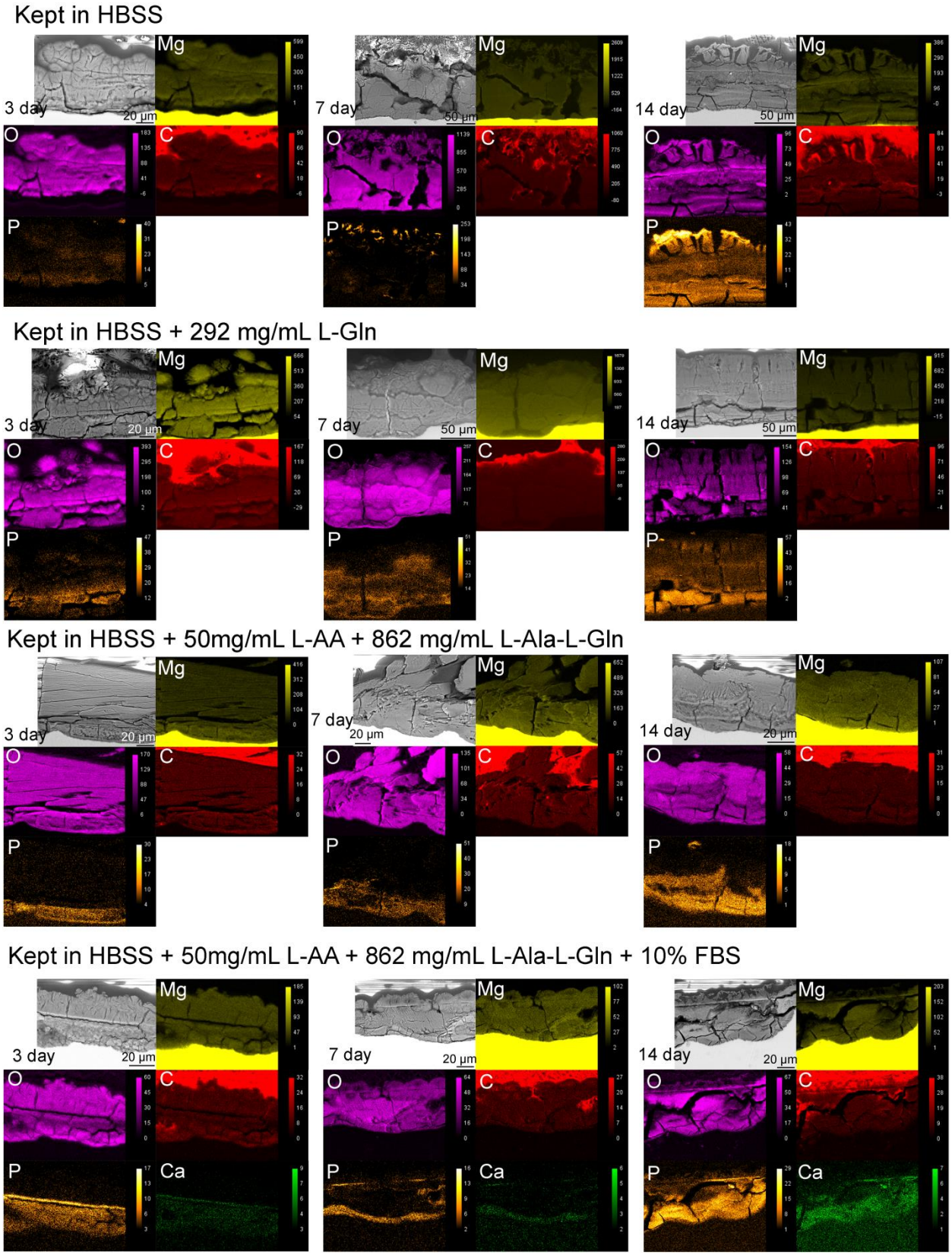
Kept in HBSS
3 day
7 day
14 day
Mg
O
C
P
Ca
20 μm
50 μm
Kept in HBSS + 292 mg/mL L-Gln
Kept in HBSS + 50mg/mL L-AA + 862 mg/mL L-Ala-L-Gln
Kept in HBSS + 50mg/mL L-AA + 862 mg/mL L-Ala-L-Gln + 10% FBS

Fig. 8

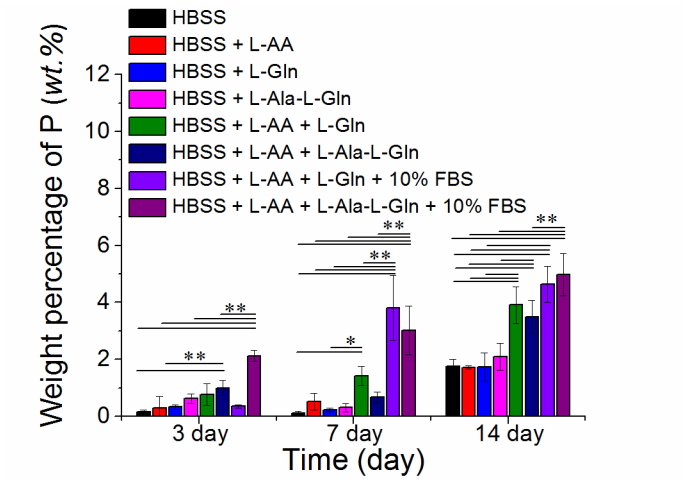
HBSS
HBSS + L-AA
HBSS + L-Gln
HBSS + L-Ala-L-Gln
HBSS + L-AA + L-Gln
HBSS + L-AA + L-Ala-L-Gln
HBSS + L-AA + L-Gln + 10% FBS
HBSS + L-AA + L-Ala-L-Gln + 10% FBS
Weight percentage of P (wt.%)
0
2
4
6
8
10
12
3 day
7 day
14 day
Time (day)
**
**
*
**
**
**

Fig. 9

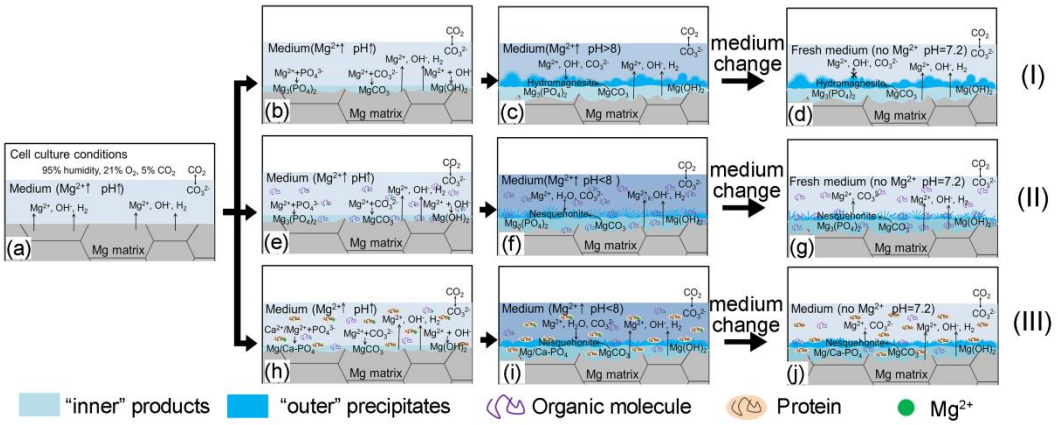
Cell culture conditions
95% humidity, 21% O2, 5% CO2
Medium (Mg2+↑ pH↑)
(a)
Mg matrix
Medium(Mg2+↑ pH↑)
(b)
Medium(Mg2+↑ pH>8)
(c)
medium change
Fresh medium (no Mg2+ pH=7.2)
(d)
(I)
Medium (Mg2+↑ pH↑)
(e)
Medium(Mg2+↑ pH<8)
(f)
Fresh medium (no Mg2+ pH=7.2)
(g)
(II)
Medium (Mg2+↑ pH↑)
(h)
Medium (Mg2+↑ pH<8)
(i)
Medium (no Mg2+ pH=7.2)
(j)
(III)
Hydromagnesite
Nesquehonite
"inner" products
"outer" precipitates
Organic molecule
Protein
Mg2+

Tables

Table 1: Chemical composition of pure Mg.

Table 2: The composition of Hanks' balanced salt solution (HBSS).

Table 1

Composition (*Wt.%*)	Ca	Zn	Fe	Cu	Si	Mn	Mg
Weight percentage	0.0004	0.018	0.0044	0.0089	0.0014	0.0021	balance

Table 2

Ingredient	mg/L	mM
Potassium chloride (KCl)	400	5.33
Potassium Phosphate monobasic (KH_2PO_4)	60	0.441
Sodium bicarbonate ($NaHCO_3$)	350	4.17
Sodium chloride (NaCl)	8000	137.93
Sodium phosphate dibasic (Na_2HPO_4 $2H_2O$) anhydrous	48	0.338
D-Glucose (Dextrose)	1000	5.56